AIAA AVIATION Forum
June 15-19, 2020, VIRTUAL EVENT
AIAA AVIATION 2020 FORUM

10.2514/6.2020-2641

Differential Dynamic Programming to Critical-Engine-Inoperative Takeoff Certification Analysis

Jiacheng Xie*, Evan D. Harrison†, and Dimitri N. Mavris‡
Aerospace Systems Design Laboratory, School of Aerospace Engineering
Georgia Institute of Technology, Atlanta, Georgia, 30332

Critical-engine-inoperative (CEI) takeoff is a required flight test in transport aircraft type certification. Due to the limited excess power following engine failure, this flight test is potentially dangerous and highly sensitive to the flight controls. To enhance the flight safety in CEI takeoff, an optimal longitudinal control sequence is necessary for the flight test. On the other hand, to reduce the cost associated with type certification process, it is desired to incorporate certification analysis in early design phases. Since the certification regulations pose requirements on aircraft dynamic responses, the point-mass based method used in most of the takeoff analyses for aircraft early design is not suitable. To incorporate flight dynamics in takeoff analysis, a robust longitudinal control law is needed for takeoff performance prediction. This paper proposes to use Differential Dynamic Programming (DDP) for the optimization of elevator control for CEI takeoff certification analysis. To evaluate the method, two test cases are performed on the CEI takeoff of a small single-aisle aircraft model with different initial conditions. The results of two cases suggests that the DDP algorithm is able to optimize the trajectory in terms of minimizing takeoff distance, maximizing the rate of climb, and improving the compliance with respect to takeoff certification constraints. The optimized trajectory is sensitive to the initial control sequence given to the algorithm and the cost function settings.

I. Nomenclature

α	=	angle of attack
β	=	sideslip angle
θ	=	pitch attitude
γ	=	flight path angle
δ_e	=	elevator defection
$\bar{c}$	=	reference chord length
C_D	=	drag coefficient
C_f	=	runway friction coefficient
C_L	=	lift coefficient
C_{m_0}	=	pitching-moment coefficient at zero angle of attack
C_{m_α}	=	pitching-moment coefficient with angle of attack
$C_{m_{\delta_e}}$	=	pitching-moment coefficient with elevator deflection
$C_{m_{\hat{q}}}$	=	pitching-moment coefficient with pitch rate
D	=	drag
I_{yy}	=	pitching mass moment of inertia
L	=	lift
P_s	=	excess power
q	=	pitch rate
S	=	reference wing area
T	=	thrust
u	=	body x-axis velocity
V_∞	=	airspeed

*Ph.D. Student, ASDL, School of Aerospace Engineering, Georgia Tech, AIAA Student Member
†Research Engineer II, ASDL, School of Aerospace Engineering, Georgia Tech, AIAA Member
‡S.P. Langley Distinguished Regents Professor and Director of ASDL, Georgia Tech, AIAA Fellow

w = body z-axis velocity
W = weight

II. Introduction

Takeoff performance is of essential importance in aircraft design. In Title 14 of the Code of Federal Regulations (14 CFR) Part-25 [1], the takeoff certification requirements are specified including takeoff speeds, takeoff distance, takeoff path, etc. To show the compliance with respect to these certification regulations, the aircraft must perform flight tests following the procedures described in the Advisory Circular [2]. One of the required flight tests is the critical-engine-inoperative (CEI) takeoff. The CEI takeoff flight test can be particularly dangerous due to the limited excess power available due to the simulated engine failure. Aircraft manufacturers want to have their aircrafts to be certified with minimized takeoff field length because it determines the takeoff operational limit which directly affects the market performance of their products. But meanwhile, the manufactures also need to guarantee the whole flight test process is safe and satisfies the regulatory requirements. Although takeoff performance is mostly determined by aircraft sizing and design, the responses of aircraft in flight test can also be significantly affected by the strategy of longitudinal control. Therefore, to encourage an optimal takeoff certification result, it is necessary to have an optimal flight control applied on the aircraft.

On the other hand, type certification is a process that is expensive, time-consuming, and subject to uncertainties [3]. In order to reduce the cost associated with certification, it is desired to incorporate certification consideration into aircraft early design phase to promote the viability of the design. Such incorporation requires a relatively accurate and robust certification analysis capability to be integrated in sizing and design loop. Because the regulations pose requirements on aircraft dynamic responses, the point-mass performance evaluation method may no longer be valid for certification analysis. Considering that takeoff performance and dynamics are sensitive to flight control, it is necessary to introduce a robust way to determine the optimal flight control in certification analysis capability, thus to better evaluate how "best" the current design can perform with respect to takeoff certification requirements.

A number of methods have been proposed for takeoff modeling. Past studies have focused on takeoff analysis for aircraft sizing and performance analysis [4–7], takeoff trajectory prediction for aircraft operational level analysis [8, 9], takeoff dynamics modeling [10–13], one-engine-out lateral path strategy [14, 15], and lateral controllability at CEI [16, 17]. Limitations in preceding research include: 1. The point-mass based method used in most research cannot capture the aircraft dynamic responses during takeoff; 2. Most of the CEI takeoff analyses ignored the takeoff climb segment from 400 to 1500 feet, but this segment could be critical to CEI flight due to limited excess power; 3. The control laws used in existing longitudinal takeoff dynamic simulations are mostly open-loop or aircraft-depended, which are not robust and cannot guarantee the optimal takeoff performance.

This paper proposes an approach to optimize the longitudinal control for CEI takeoff using Differential Dynamic Programming (DDP) [18], thus to improve the takeoff certification analysis capability. The reminder of this paper is organized as follows: Section III describes the takeoff flight dynamics modeling; Section IV introduces the method and algorithm of the DDP; Section V discusses how the DDP is applied to the CEI takeoff trajectory optimization; Section VI presents the CEI takeoff simulation and optimization results of the test cases; Section VII draws some conclusions from the presented results.

III. Takeoff Dynamics Modeling

The takeoff dynamic simulation is performed on the Flight Certification Analysis Module [19] developed in Georgia Tech Aerospace Systems Design Laboratory. Suppose that the side force and yawing moment from inoperative engine are balanced by steady sideslip and rudder control, and assume no lateral or directional motions, the takeoff process can be regarded as a three degree-of-freedom longitudinal dynamics. Assuming the body axes aligned with the principle

axes for simplification, the equations of motion are written as:

$$\begin{cases} \dot{u} = X/m - g\sin\theta - qw \\ \dot{w} = Z/m + g\cos\theta + qu \\ \dot{q} = M/I_{yy} \\ \dot{\theta} = q \\ \dot{x}_e = u\cos\theta - w\sin\theta \\ \dot{z}_e = u\sin\theta + w\cos\theta \end{cases} \tag{1}$$

where X, Z, and M are the external forces and moment contributed by aerodynamics, propulsion, and ground roll, measured in aircraft body axes. The expressions for these forces and moments are explained later. x_e and z_e are the displacements in ground axes, i.e. the takeoff horizontal distance and altitude above the ground.

The takeoff simulation follows the procedure described in the Advisory Circular AC 25-7D [2] as shown in Fig. 1. The process can be divided into two segments: the ground roll before lift-off and the takeoff climb after lift-off.

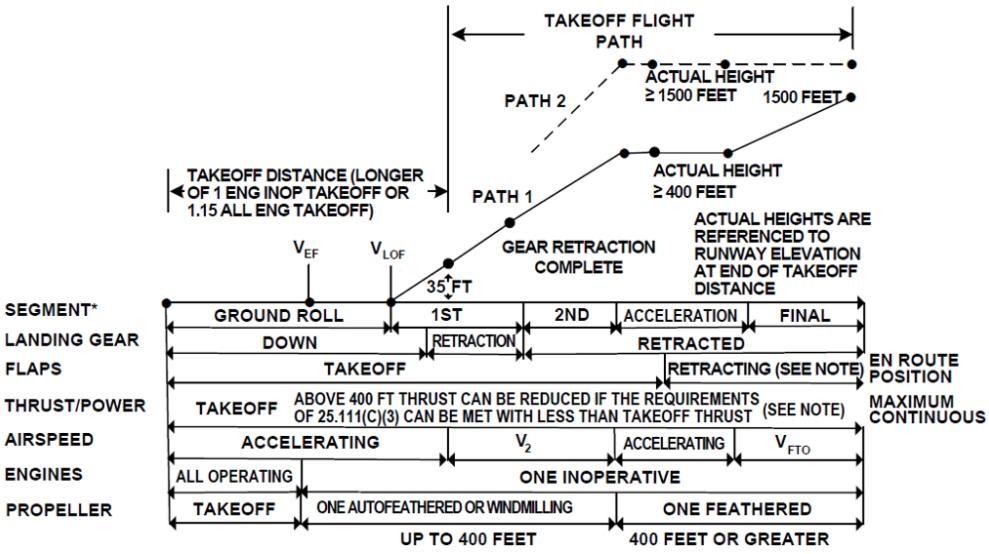

Fig. 1 Takeoff Segments and Nomenclature [2]

The ground roll segment includes all-engine-operating accelerating to V_{EF}, critical engine failure at V_{EF}, critical-engine-inoperative accelerating to decision speed V_1, rotating at V_R, and accelerating to lift-off speed V_{LOF}. In this paper, V_{EF} and V_1 are given externally and remained fixed in the optimization process. The external forces and pitch moment at ground roll segment are given by

$$X = T + X_{aero} + X_{ground} \tag{2}$$

$$Z = Z_{aero} + Z_{ground} \tag{3}$$

$$M = M_{aero} + M_{thrust} + M_{ground} \tag{4}$$

In these equations, the aerodynamic forces and moment are given by

$$\begin{cases} L = \frac{1}{2}\rho V_\infty^2 S C_L \\ D = \frac{1}{2}\rho V_\infty^2 S C_D \end{cases} \tag{5}$$

$$\begin{cases} X_{aero} = -D\cos\alpha\cos\beta + L\sin\alpha \\ Z_{aero} = -L\cos\alpha - D\cos\beta\sin\alpha \\ M_{aero} = \frac{1}{2}\rho V_\infty^2 S\bar{c}(C_{m_0} + C_{m_\alpha}\alpha + C_{m_{\hat{q}}}\hat{q} + C_{m_{\delta_e}}\delta_e) \end{cases} \tag{6}$$

where C_L and C_D are varying with angle of attach α and elevator deflection δ_e. The sideslip β is computed from lateral trim and assumed constant after V_1. The ground forces and moment are given by:

$$\begin{cases} X_{ground} = -C_f(W-L)\cos\alpha\cos\beta - (W-L)\sin\alpha \\ Z_{ground} = -(W-L)\cos\alpha - C_f(W-L)\cos\beta\sin\alpha \\ M_{ground} = -(W-L)(x_{MW}-x_{CG}) - C_f(W-L)(z_{CG}-z_{MW}) \end{cases} \tag{7}$$

where x_{CG} (z_{CG}) and x_{MW} (z_{MW}) are the x(z)-coordinates of center of gravity and main landing gear measured from aircraft front-nose. The pitching moment from thrust is given by:

$$M_{thrust} = T \cdot z_N \tag{8}$$

where z_N is the vertical distance between nacelle main axis and aircraft main axis.

The takeoff climb segment is from the lift-off to 1500 feet above ground. The forces and pitch moment at this segment are governed by:

$$X = T + X_{aero} \tag{9}$$

$$Z = Z_{aero} \tag{10}$$

$$M = M_{aero} + M_{thrust} \tag{11}$$

where the aerodynamic forces and moment are given by Eqs. (5) (6), and the pitch moment from thrust is given by Eq. (8).

In this paper, the dynamic simulation is performed in discretized time domain. The state variables are iteratively updated by numerically solving the equations of motion using the Euler's method. The control variable is determined and optimized by the Differential Dynamic Programming introduced in following section.

IV. Differential Dynamic Programming

Differential Dynamic Programming (DDP) is an optimum control algorithm for trajectory optimization [18]. For a discrete dynamics $\mathbf{x}_{i+1} = \mathbf{f}(\mathbf{x}_i, \mathbf{u}_i)$ (such as the takeoff dynamics governed by Eq. (1)), the cost function for a finite horizon spanning from initial state to final time step N can be written as:

$$J_0(\mathbf{x}, \mathbf{U}) = \sum_{i=0}^{N-1} g(\mathbf{x}_i, \mathbf{u}_i) + g_f(\mathbf{x}_N) \tag{12}$$

where $\mathbf{U}$ is the control sequence from initial state to final state, g is the cost at each time step, and g_f is the terminal cost at the end point. The value function is defined as the minimization of cost function with the optimal control sequence and written as a function of state variables:

$$V(\mathbf{x}, 0) = \min_{\mathbf{U}} J_0(\mathbf{x}, \mathbf{U}) \tag{13}$$

In the DDP, the optimal control problem is decomposed into a series of recursive subproblems and iteratively solved backward in time by the Bellman equation. The Bellman equation describes the relationship between the value function in one time step and the value function in the next time step:

$$V(\mathbf{x}, i) = \min_{\mathbf{u}}[g(\mathbf{x}, \mathbf{u}) + V(\mathbf{f}(\mathbf{x}, \mathbf{u}), i+1)] \tag{14}$$

This implies that if the optimization is worked backwards, the value function at time step i can be found from the value function at time step $i+1$. Perturbing the value function around (x, u) at time step i, and letting Q be the variation of value function yields:

$$Q(\delta\mathbf{x}, \delta\mathbf{u}) = g(\mathbf{x}+\delta\mathbf{x}, \mathbf{u}+\delta\mathbf{u}) - g(\mathbf{x}, \mathbf{u}) + V(\mathbf{f}(\mathbf{x}+\delta\mathbf{x}, \mathbf{u}+\delta\mathbf{u}), i+1) - V(\mathbf{f}(\mathbf{x}, \mathbf{u}), i+1) \tag{15}$$

Expanding Q with second-order approximation and denote V' as the value function at next time step $V(i+1)$:

$$Q(\delta\mathbf{x}, \delta\mathbf{u}) = Q_{\mathbf{x}}\delta\mathbf{x} + Q_{\mathbf{u}}\delta\mathbf{u} + \frac{1}{2}\delta\mathbf{x}^T Q_{\mathbf{xx}}\delta\mathbf{x} + \frac{1}{2}\delta\mathbf{u}^T Q_{\mathbf{uu}}\delta\mathbf{u} + \delta\mathbf{u}^T Q_{\mathbf{ux}}\delta\mathbf{x} \tag{16}$$

where

$$\begin{cases} Q_{\mathbf{x}} = g_{\mathbf{x}} + \mathbf{f}_{\mathbf{x}}^T V_{\mathbf{x}}' \\ Q_{\mathbf{u}} = g_{\mathbf{u}} + \mathbf{f}_{\mathbf{u}}^T V_{\mathbf{x}}' \\ Q_{\mathbf{xx}} = g_{\mathbf{xx}} + \mathbf{f}_{\mathbf{x}}^T V_{\mathbf{xx}}' \mathbf{f}_{\mathbf{x}} + V_{\mathbf{x}}' \cdot \mathbf{f}_{\mathbf{xx}} \\ Q_{\mathbf{uu}} = g_{\mathbf{uu}} + \mathbf{f}_{\mathbf{u}}^T V_{\mathbf{xx}}' \mathbf{f}_{\mathbf{u}} + V_{\mathbf{x}}' \cdot \mathbf{f}_{\mathbf{uu}} \\ Q_{\mathbf{ux}} = g_{\mathbf{ux}} + \mathbf{f}_{\mathbf{u}}^T V_{\mathbf{xx}}' \mathbf{f}_{\mathbf{x}} + V_{\mathbf{x}}' \cdot \mathbf{f}_{\mathbf{ux}} \end{cases} \tag{17}$$

By minimizing $Q(\delta\mathbf{x}, \delta\mathbf{u})$ with respect to $\delta\mathbf{u}$ and ignoring the second-order tensor contractions in $Q_{\mathbf{xx}}$, $Q_{\mathbf{uu}}$, and $Q_{\mathbf{ux}}$, the optimal change in control is computed as

$$\delta\mathbf{u}^* = -Q_{\mathbf{uu}}^{-1} Q_{\mathbf{u}} - Q_{\mathbf{uu}}^{-1} Q_{\mathbf{ux}} \delta\mathbf{x} = \mathbf{k} + \mathbf{K}\delta\mathbf{x} \tag{18}$$

Substituting $\delta\mathbf{u}^*$ back to Q, the local quadratic approximation of the variation of value function at time step i becomes

$$\Delta V(i) = -\frac{1}{2} Q_{\mathbf{u}} Q_{\mathbf{uu}}^{-1} Q_{\mathbf{u}} \tag{19}$$

$$V_{\mathbf{x}}(i) = Q_{\mathbf{x}} - \mathbf{K}^T Q_{\mathbf{uu}} \mathbf{k} \tag{20}$$

$$V_{\mathbf{xx}}(i) = Q_{\mathbf{xx}} - \mathbf{K}^T Q_{\mathbf{uu}} \mathbf{K} \tag{21}$$

The general steps of DDP to discrete dynamics control optimization are as follows [20]:

1) **Initialization**: Start with an initial trajectory with nominal control and state variables. For each time step, compute partial derivatives of cost and dynamics with respect to state and control: $g_{\mathbf{x}}$, $g_{\mathbf{u}}$, $g_{\mathbf{xx}}$, $g_{\mathbf{uu}}$, $g_{\mathbf{ux}}$, $\mathbf{f}_{\mathbf{x}}$, $\mathbf{f}_{\mathbf{u}}$, $\mathbf{f}_{\mathbf{xx}}$, $\mathbf{f}_{\mathbf{uu}}$, $\mathbf{f}_{\mathbf{ux}}$.
2) **Backward sweep**: Along the trajectory, compute the local quadratic approximation of the value function $V(\mathbf{x}, i)$ at each time step from the end point $i = N$ to the starting point $i = 0$ using Eqs. (15) to (21).
3) **Forward sweep**: Compute the new optimized control using Eq. (18), and re-launch the dynamic simulation to compute the new trajectory as well as the partial derivatives of cost and dynamics with respect to state and control
4) **Iteration**: Repeat the backward sweep and forward sweep until the value function and trajectory converge to the optimal solution.

V. Takeoff Trajectory Optimization

A. Objectives and Constraints

The goal of the takeoff trajectory optimization is to find the optimal elevator control law for the dynamic simulation of CEI takeoff certification using the DDP. The objectives of the optimization includes minimizing takeoff distance, minimizing the time to climb, and maximizing flight safety margin. Minimizing takeoff distance is to minimize the horizontal distance from starting point to 35 feet above ground according to 14 CFR 25.113 [1].Minimizing the time to climb is to maximize the rate of climb at each point of takeoff trajectory. As for the flight safety margin, two aspects are considered. One is to maximize the excess power. Higher excess power means the aircraft is being operated further away from limits, which gives more tolerance on the pilot control actions and allows the aircraft to climb faster. For a fixed-design aircraft, although the maximum available excess power is determined by its aerodynamic, weight, and propulsion characteristics, the actual excess power in unsteady flight can be significantly varied by the flight control. Another way to maximize safety margin is to minimize the control efforts. The certification rule requires that all the flight tests should be performed by average pilot skills, so the optimized control sequence should not include any rapid change in control or any extreme movement applied on the control stick. Frequent and rapid changes on elevator control may not only be out of pilot's skill, but also cause structural fatigue to the control surfaces.

The constraints associated with the trajectory optimization include the certification rules from 14 CFR Part-25 Subpart-B Flight [1]. The takeoff speed constraints are specified in 14 CFR 25.107 [1], including $V_R \geq \max(V_1, 1.05V_{MC})$, $V_2 \geq \max(1.13V_{SR}, 1.1V_{MC})$, and $V_{FTO} \geq 1.18V_{SR}$. The gradient of climb ($\tan\gamma$) constraints are specified in 14 CFR 25.111 and 25.121 [1], including $\tan\gamma \geq 0$ at lift-off, $\tan\gamma \geq 0.024$ at landing gear retraction, and $\tan\gamma \geq 0.012$ between 400 feet and 1500 feet (for two-engine aircraft) .

B. DDP Optimization

Suppose $\mathbf{x} = [u, w, q, \theta, x_e, z_e]^T$ and $\mathbf{u} = \delta_e$, the DDP takeoff trajectory optimization can be written as:

$$\begin{aligned} \min_{\mathbf{U}} \quad & J_0(\mathbf{x}, \mathbf{U}) \\ \text{s.t.} \quad & \dot{\mathbf{x}} = \mathbf{f}(\mathbf{x}, \mathbf{u}) \\ & \delta_{e_{min}} \leq \mathbf{u} \leq \delta_{e_{max}} \end{aligned} \tag{22}$$

where $\mathbf{f}(\mathbf{x}, \mathbf{u})$ is the takeoff dynamic function from Eq. (1). $\delta_{e_{min}}$ and $\delta_{e_{max}}$ are the elevator upward and downward deflection limits. In this paper, the elevator travel range is assumed between $-30°$ and $30°$.

The core of the DDP algorithm is to define the cost function $J_0(\mathbf{x}, \mathbf{U})$ appropriately such that by minimizing the cost, the optimized trajectory could be pushed toward the objectives while satisfying constraints. As described in Sec. IV, the cost function involves two terms: the cost at each time step g and the terminal cost g_f. This paper defines three costs g at different segments of takeoff and one terminal cost g_f at the end of trajectory.

The first cost $g_1(\mathbf{x}, \mathbf{u})$ is applied to the segment between starting point and 35 feet above ground and defined as a function of climb angle and control change:

$$g_1(\mathbf{x}, \mathbf{u}) = R_\gamma \frac{1}{\bar{\gamma} + \epsilon} + \frac{1}{2} \Delta \mathbf{u}^T R_\mathbf{u} \Delta \mathbf{u} \tag{23}$$

where $\bar{\gamma}$ is the normalized climb angle:

$$\bar{\gamma} = \frac{\gamma}{\gamma_{\max}} \tag{24}$$

$$\gamma = \theta - \arctan \frac{w}{u} \tag{25}$$

R_γ and $R_\mathbf{u}$ are the weight factors corresponding to the terms of climb angle and control change. ϵ is to prevent the denominator of inverse term from being less or equal to zero. The goal of $g_1(\mathbf{x}, \mathbf{u})$ is to maximum the climb angle to clear the obstacle and satisfy the gradient of climb constraint at 35 feet. By setting climb angle term inversely, the aim is to minimize the takeoff distance since the zero γ at ground roll would largely increase the cost.

The second cost $g_2(\mathbf{x}, \mathbf{u})$ is applied to the segment between 35 and 400 feet above ground and defined as a function of climb angle, excess power, and control change:

$$g_2(\mathbf{x}, \mathbf{u}) = R_\gamma \frac{1}{\bar{\gamma} + \epsilon} + R_{P_s} \frac{1}{\bar{P}_s + \epsilon} + \frac{1}{2} \Delta \mathbf{u}^T R_\mathbf{u} \Delta \mathbf{u} \tag{26}$$

where $\bar{P}_s$ is the normalized excess power:

$$\bar{P}_s = \frac{P_s}{P_{s_{\max}}} \tag{27}$$

$$P_s = V_\infty \sin\gamma + \frac{V_\infty}{g} \frac{dV_\infty}{dt} \tag{28}$$

$$V_\infty = \sqrt{u^2 + w^2} \tag{29}$$

R_{P_s} is the weight factor corresponding to excess power. The goal of $g_2(\mathbf{x}, \mathbf{u})$ is to keep the maximum climb angle from obstacle clearance as indicated by Fig. 1 while maintaining sufficient excess power for takeoff speed constraints and flight safety consideration.

The third cost $g_3(\mathbf{x}, \mathbf{u})$ is applied to the segment between 400 and 1500 feet above ground and defined as a function of rate of climb, climb angle, excess power, and control change:

$$g_3(\mathbf{x}, \mathbf{u}) = R_{RoC} \frac{1}{R\bar{o}C + \epsilon} + R_\gamma \frac{1}{\bar{\gamma} + \epsilon} + R_{P_s} \frac{1}{\bar{P}_s + \epsilon} + \frac{1}{2} \Delta \mathbf{u}^T R_\mathbf{u} \Delta \mathbf{u} \tag{30}$$

where $R\bar{o}C$ is the normalized rate of climb:

$$R\bar{o}C = \frac{V_\infty \sin\gamma}{(V_\infty \sin\gamma)_{max}} \tag{31}$$

R_{RoC} is the weight factor corresponding to rate of climb. The goal of $g_3(\mathbf{x}, \mathbf{u})$ is to minimize the time to climb while satisfying the minimum gradient of climb constraint between 400 and 1500 feet from 14 CFR 25.111 and maintaining the flight safety margin.

The terminal cost g_f at the end point is defined as the deviation from expected final state $\mathbf{x}_{target}$ and the terminal state computed from dynamic simulation $\mathbf{x}_N$:

$$g_f(\mathbf{x}_N) = \frac{1}{2}(\mathbf{x}_N - \mathbf{x}_{target})^T R_{\mathbf{x}_N}(\mathbf{x}_N - \mathbf{x}_{target}) \tag{32}$$

where R_{x_N} is the weight matrix for the terminal cost function. In this paper, the target state is selected as the maximum rate of climb trimmed condition at 1500 feet, which is to push the aircraft to successfully climb to 1500 feet as required by the regulation while minimizing the time to climb. This target state is computed at the beginning of optimization using trim analysis and fixed in iteration process.

With $g(\mathbf{x}, \mathbf{u})$ and $g_f(\mathbf{x}_N)$ defined, the cost function $J(\mathbf{x}, \mathbf{U})$, the value function $V(\mathbf{x}, i)$, and the local variation of value function $Q(\delta\mathbf{x}, \delta\mathbf{u})$ can be found from Eqs. (12) (14) (15). The optimal longitudinal control is solved through the four steps of DDP described in Sec. IV. The derivatives of $\mathbf{f}(\mathbf{x}, \mathbf{u})$, $g(\mathbf{x}, \mathbf{u})$, and $g_f(\mathbf{x}_N)$ are computed numerically using the central-differential scheme. The optimization algorithm flowchart is illustrated in Fig. 2.

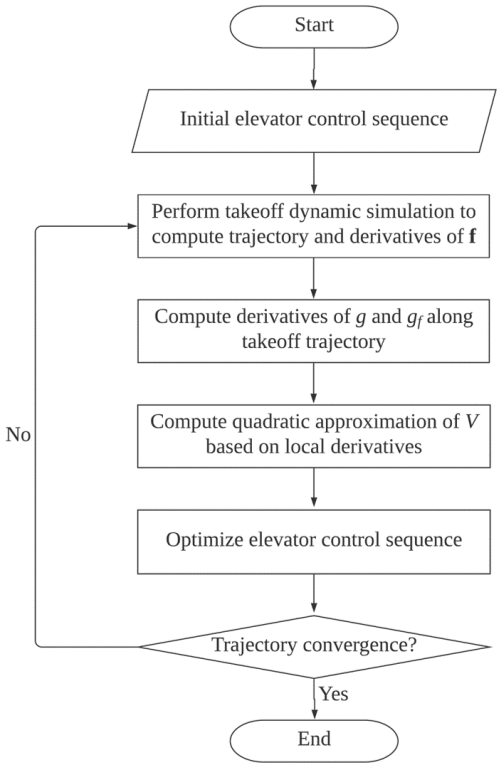

Fig. 2 CEI Takeoff Trajectory Optimization Algorithm

VI. Test Cases

To demonstrate the method, this paper applies the DDP algorithm to the critical-engine-inoperative takeoff of a small single-aisle aircraft (SSA) model. The SSA model is sized by the Environmental Design Space (EDS) [21] and calibrated using the data of Boeing 737-800 from public domain [22]. The stability and control derivatives of the SSA model are computed by the open-source vortex lattice solver AVL [23]. The key performance and geometry specifications of the SSA model are shown in Table 1 in the Appendix. The details about the SSA model development is included in Ref. [19, 24].

A. Test Case 1

The first test case starts with the initial control sequence of zero elevator deflections. The optimization results of the test case are included in Fig. 3 and Fig. 4.

Fig. 3 shows the CEI takeoff trajectories and elevator control sequences from initial condition to 100 iteration steps of applying the DDP. The blue dash curve represents the initial trajectory and control sequence, and the light blue curve represents the final optimized solution at 100 iteration steps, while the other curves represent the trajectory and control sequence at intermediate optimization steps. Comparing the optimized controls with the initial condition in the control sequence plot, the main difference is that the elevator is deflected to almost the upward limit right after V_R and then recovered back during the rotating process until lift-off. This accelerates the takeoff rotation which in turn makes the lift-off much earlier than the initial case as shown in the trajectory plot.

For the details along the trajectory, Fig. 4 tracks the changes of takeoff distance, takeoff speeds, rate of climb, and gradients of climb at each optimization step. It is seen that the takeoff distance is successfully decreased in the optimization and converge at 10 947 feet. The rate of climb at the end point is dropped at the first step but then monotonically increased in the optimization process due to target state $\mathbf{x}_{target}$ setting and the inverse term of rate of climb defined in cost g_3. As a result, the rate of climb at 1500 feet in optimized trajectory is higher than that in the initial condition.

The takeoff certification constraints mentioned in Sec. V.A are also examined in the iteration as indicated by the history plots of gradient of climb and takeoff speeds. The available gradient of climb constraint is checked at 35 feet as required by §25.121 and the minimum gradient of climb constraint is checked between 400 and 1500 feet as required by §25.111. The dash lines in the gradient of climb history plots represent the minimum constraint values defined in these regulations. Note that the gradient of climb constraints are initially violated, but soon mitigated in the optimization. Regarding the takeoff speeds constraints, the test case tracks the changes of V_2 and V_{FTO} during the optimization process. V_2 is decreased in the optimization because the shorter takeoff ground roll optimized by cost g_1 makes the aircraft lift off at a lower speed. V_{FTO} is increased in the optimization because excess power and rate of climb are maximized by the inverse terms defined in g_2 and g_3 which promotes the acceleration during the takeoff climb segment. The constraints of V_2 and V_{FTO} are specified in §25.107 in which V_2 should be no less than $1.13V_{SR}$ and $1.1V_{mc}$, and V_{FTO} should be no less than $1.18V_{SR}$. Substituting V_{SR} and V_{mc} from Table 1, the constraint value for V_2 and V_{FTO} are 126.65 and 132.25 knots respectively. Because these constraint values are much lower than the V_2 and V_{FTO} at each iteration step, they are not included in takeoff speed history plots.

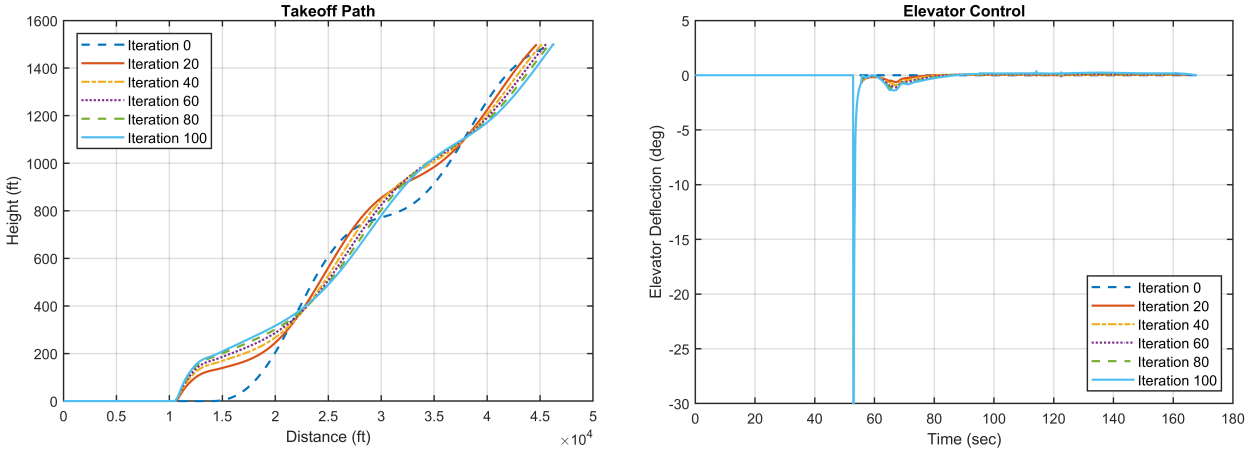

(a) Takeoff Trajectory

(b) Control Sequence

Fig. 3 Takeoff Trajectories and Control Sequences at Different Optimization Steps of Test Case 1

B. Test Case 2

Although the DDP successfully minimizes the takeoff distance for the first test case, the final optimal solution converged at 10.947 feet is still higher than the takeoff distance 7780 feet of B737-800 documented in public domain. This is due to the limitation of the DDP algorithm in takeoff trajectory optimization: the control optimization can only

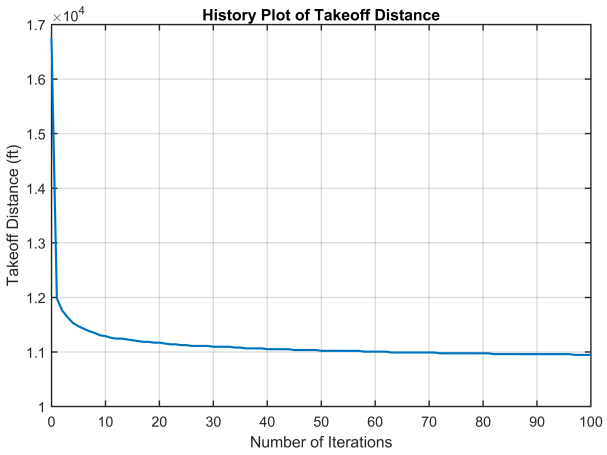

(a) Takeoff Distnace

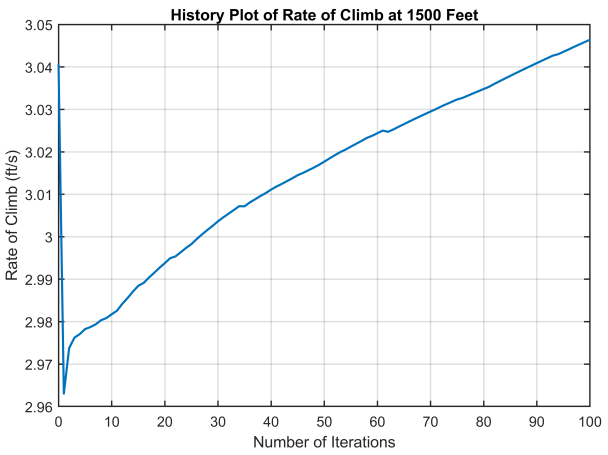

(b) Rate of Climb at Takeoff End point

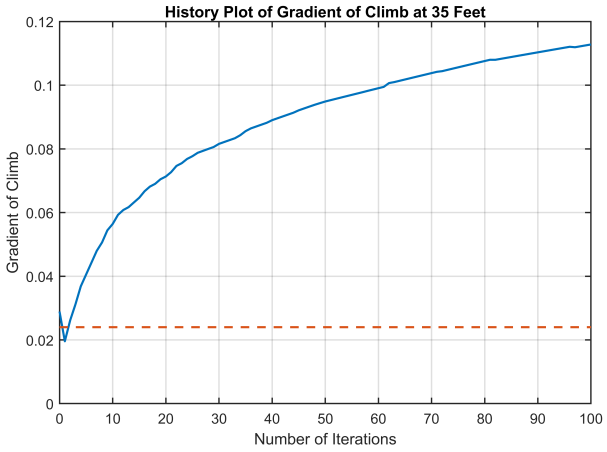

(c) 35 ft Gradient of Climb

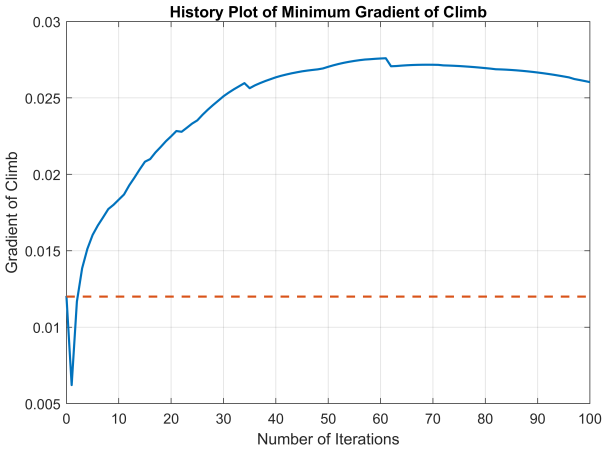

(d) Minimum Gradient of Climb between 400 and 1500 ft

(e) Takeoff Safety Speed V_2

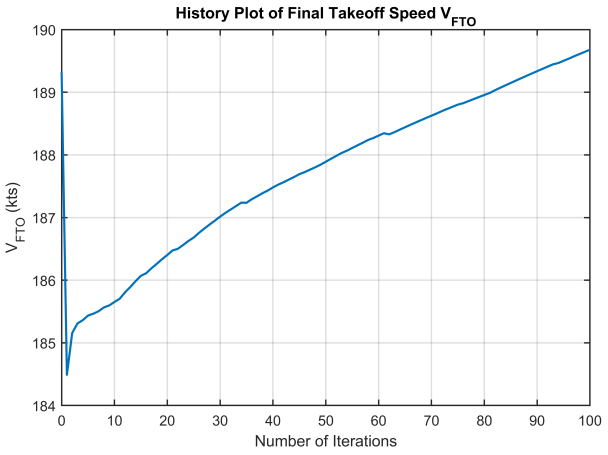

(f) Final Takeoff Speed V_{FTO}

Fig. 4 Takeoff Objectives and Constraints Tracking in Optimization Process of Test Case 1

start after the takeoff rotation at V_R but it cannot move the rotation point forward or backward because the derivatives $\mathbf{f_u}$, $g_\mathbf{u}$, $g_\mathbf{uu}$, and $g_\mathbf{ux}$ are always zero before the rotation which makes Eq. (18) equal to zero. To solve the problem, this paper launched another test case with a new initial control sequence of constant -3 deg, which decreases the V_R from 175 knots of first test case to 148 knots.

The DDP optimization results of the second test case are included in Fig. 5 and Fig. 6. The number of iterations of the second case is increased from 100 of the first case to 300 because this case is more difficult to converge. The general trend of the optimized elevator control sequences are similar to the first test case with significant upward deflection after V_R and slight control change during takeoff climb, as shown Fig. 5. Note that there is an abrupt jump around the end point, and this might be caused by the terminal cost g_f and associated derivatives since the g_f tends to push the aircraft to match the velocity and pitch angle at the maximum rate of climb trim condition. For the trajectory, similar to the first test case, the lift-off point is moved forward in optimized trajectory. But when comparing the optimized trajectories of two test cases shown in Fig. 3 and Fig. 5, it is found that the initial takeoff climb path from ground to about 100 feet height is much flatter in case 2 than that in case 1. The degraded climb gradient might be due to the difference in ground roll distance. Earlier lift-off may encourage shorter takeoff distance, but the shorter ground-roll acceleration may not be able to provide the aircraft enough mechanical energy to support a higher climb angle. Therefore, the optimized trajectory of case 2 has a shorter takeoff distance, but the initial takeoff climb gradient is higher in case 1.

Fig. 6 includes the tracking of takeoff metrics at each iteration step. As expected, the takeoff distance is minimized and rate of climb at 1500 feet is maximized, but the trends of their changes during the iteration is different from the first test case and present some "stepwise" manners. In terms of certification constraints, there are some issues happened with the constraints of gradient of climb. The gradient of climb at 35 feet is significantly decreased at first 136 steps which makes the final optimized trajectory violate the certification constraint, even though it starts recover back after step 136. But on the other hands, the minimum gradient of climb between 400 and 1500 feet shows the opposite: the optimization successfully mitigates initial constraint violation and make final optimized trajectory pass the constraint, even though there is a drop from step 52 to step 136. As for the takeoff speeds, V_2 is decreased while V_{FTO} is increased in the optimization, both of them satisfy the constraint at each iteration step. Compared to the first case, the magnitudes of V_2 and V_{FTO} are smaller and the trend of takeoff speed changes during the iteration is less continuous.

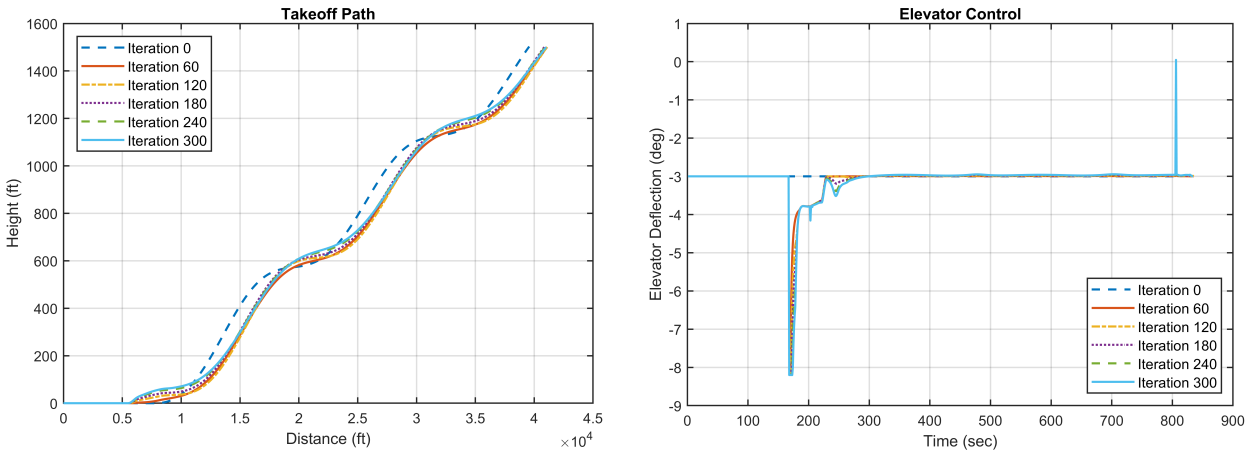

(a) Takeoff Trajectory

(b) Control Sequence

Fig. 5 Takeoff Trajectories and Control Sequences at Different Optimization Steps of Test Case 2

VII. Conclusion

This paper proposes a control optimization method for critical-engine-inoperative takeoff certification analysis using the Differential Dynamic Programming. The test cases performed in this paper demonstrate that the DDP algorithm is able to provide an optimal elevator control sequence for CEI takeoff in terms of minimizing takeoff distance, maximizing rate of climb, and improving the compliance with respect to gradient of climb and takeoff speed certification constraints. The comparison between two test cases illustrates that the trajectory optimization is sensitive to the initial control sequence settings and the way to define the cost function. Future investigation will be conducted to evaluate how

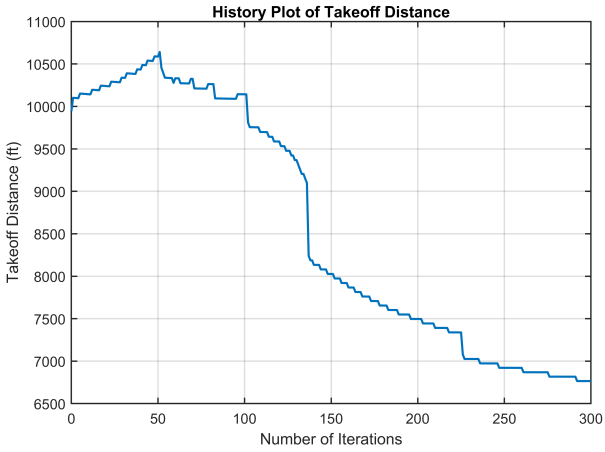

(a) Takeoff Distnace

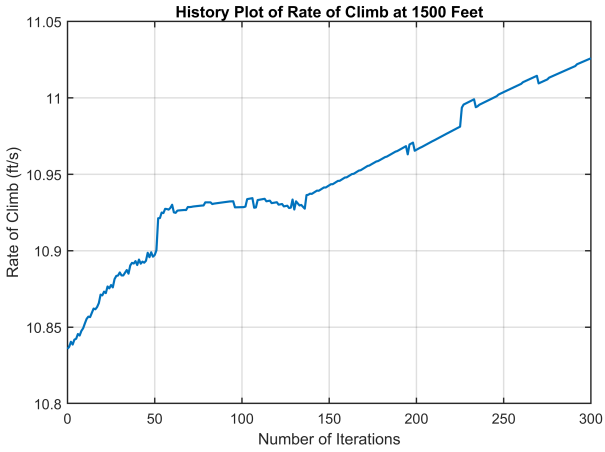

(b) Takeoff Safety Speed V_2

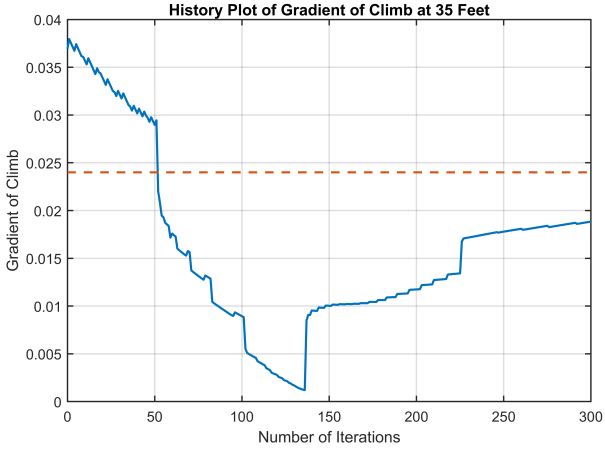

(c) 35 ft Gradient of Climb

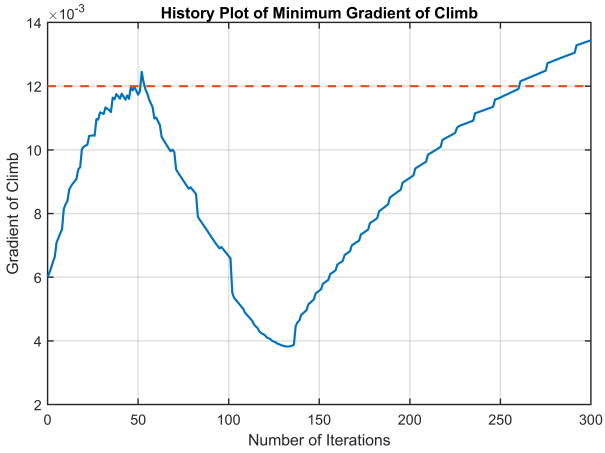

(d) Minimum Gradient of Climb between 400 and 1500 feet

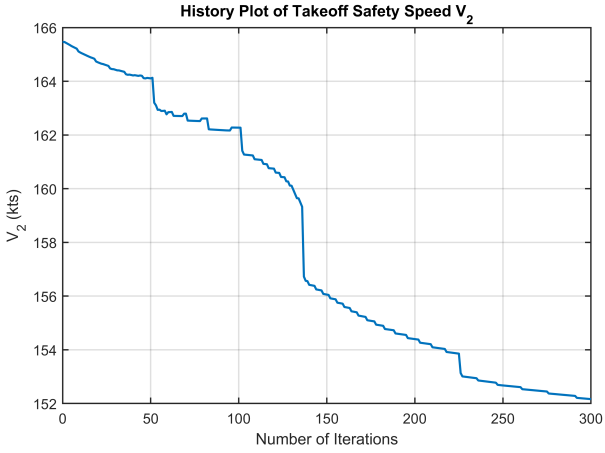

(e) 1500 ft Gradient of Climb

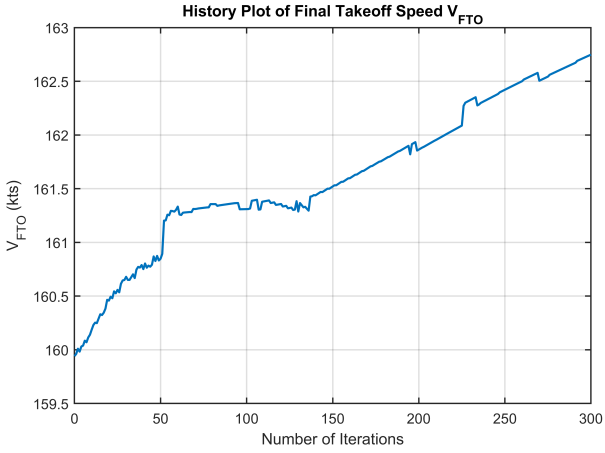

(f) Final Takeoff Speed V_{FTO}

Fig. 6 Takeoff Objectives and Constraints Tracking in Optimization Process of Test Case 2

these parameters affect the optimization and how to set these parameters appropriately to promote the convergence and encourage a more optimal control sequence.

The application of the DDP to CEI takeoff certification analysis provides an insight of implementing machine-learning techniques to enhance aircraft virtual certification. The goal of virtual certification includes two aspects: 1. Certification by analysis: Move some of the flight tests and ground experiments to digital platform thus to reduce cost and time spent on certification process; 2. Certification driven design: Provide certification predictions using simulation and analysis in early design phases to improve the robustness of a new design. In terms of certification by analysis, by integrating the machine-learning techniques like the DDP into digital platforms, some alternative and potentially more optimal flight test strategies could be explored and virtually tested without taking risks in real flight test, and thus further "exploit" the performance of aircraft and improve the flight safety. As for certification driven design, the incorporation of certification analysis in aircraft early design allows the certification constraints to be quantified in conceptual level, but such incorporation might be impeded by the lack of design knowledge in early design phases. However, machine-learning techniques may help with overcome such obstacles. For instance, the DDP method presented in this paper shows an example of performing dynamic simulation and trajectory optimization without knowing the detailed design knowledge of aircraft control systems. Potentially, it can be expected that such manner of integrating machine-learning techniques with certification analysis could be applied to other disciplines and other sections of certification rules. Future work will further explore the benefits of implementing machine-learning techniques in aircraft virtual certification.

Appendix

Table 1 Specifications of Small Single-Aisle Aircraft Model

Parameter	Value	Unit
Passenger capacity	160	-
Design range	3140	nmi
Cruise Mach number	0.85	-
Maximum ramp weight	174 870	lb
Maximum landing weight	146 300	lb
Sea-level static thrust	$2 \times 27\,297$	lb
Stall speed at takeoff configuration V_{SR}	112.08	kts
Minimum control speed V_{mc}	108.13	kts
Minimum control speed on ground V_{mcG}	91.72	kts
Engine failure speed V_{EF}	130.67	kts
Decision speed V_1	132.45	kts
Wing planform area	1408.5	ft^2
Wingspan	113.15	ft
Mean aerodynamic chord	11.85	ft
Wing aspect ratio	9.74	-
Wing taper ratio	0.28	-
Wing 1/4-chord sweep	25.72	deg
Wing dihedral	5.69	deg
Aileron chord ratio	0.15	-
Aileron locations (fraction of semi-span)	0.62; 0.83	-
Fuselage total length	124.75	ft
Maximum fuselage width	12.33	ft
Maximum fuselage height	13.17	ft
Horizontal tail planform area	359.22	ft^2
Horizontal tail aspect ratio	6.27	-
Horizontal tail taper ratio	0.20	-
Horizontal tail 1/4-chord sweep	29.91	deg
Elevator chord ratio	0.25	-
Elevator locations (fraction of semi-span)	0.06; 1.00	-
Vertical tail planform area	277.76	ft^2
Vertical tail aspect ratio	1.92	-
Vertical tail taper ratio	0.28	-
Vertical tail 1/4-chord sweep	35.00	deg
Rudder chord ratio	0.25	-
Rudder locations (fraction of semi-span)	0.05; 0.98	-

References

[1] *Code of Federal Regulations, Title 14, Federal Aviation Regulations, Part 25 - Airworthiness Standards: Transport Category Airplanes*, Federal Aviation Administration, 2019. URL https://www.ecfr.gov/cgi-bin/text-idx?SID=01562231188568 0c5924c66bdbc66b2c&mc=true&node=pt14.1.25&rgn=div5.

[2] *Advisory Circular AC 25-7D Flight Test Guide for Certification of Transport Category Airplanes*, Federal Aviation Administration, May 2018. URL https://www.faa.gov/documentLibrary/media/Advisory_Circular/AC_25-7D.pdf.

[3] Solar, D., "Aircraft Certification and Simulation — Current Practice, Future Outlooks and Challenges," , Sep. 2014. URL http://airtn.eu/wp-content/uploads/2_airtn-nextgen-certification-and-simulation.pdf.

[4] Raymer, D., *Aircraft Design: A Conceptual Approach, Fifth Edition*, American Institute of Aeronautics and Astronautics, Inc., 2012. doi:10.2514/4.869112.

[5] Mattingly, J. D., Heiser, W. H., and Pratt, D. T., *Aircraft Engine Design, Second Edition*, American Institute of Aeronautics and Astronautics, 2002. doi:10.2514/4.861444.

[6] Roskam, D. J., *Airplane Design Part VII: Determination of Stability, Control and Performance Characteristics (Volume 7)*, Design, Analysis and Research Corporation (DARcorporation), 2002.

[7] McCullers, L., *Flight Optimization System, Release 8.11, User's Guide*, NASA Langley Research Center, Hampton, VA 23681-0001, Oct. 2009.

[8] Lymperopoulos, I., Lygeros, J., and Lecchini, A., "Model Based Aircraft Trajectory Prediction During Takeoff," *AIAA Guidance, Navigation, and Control Conference and Exhibit*, American Institute of Aeronautics and Astronautics, 2006. doi:10.2514/6.2006-6098.

[9] Lim, D., LeVine, M. J., Ngo, V., Kirby, M., and Mavris, D. N., "Improved Aircraft Departure Modeling for Environmental Impact Assessment," *2018 Aviation Technology, Integration, and Operations Conference*, American Institute of Aeronautics and Astronautics, 2018. doi:10.2514/6.2018-3503.

[10] LOOMIS, J., "Optimal longitudinal control for obstacle clearance on takeoff," *Guidance, Control and Flight Mechanics Conference*, American Institute of Aeronautics and Astronautics, 1970. doi:10.2514/6.1970-963.

[11] Kim, M., and Kim, J., "Improved method of analyzing takeoff/landing performance of turboprop aircraft through modeling and simulation," *AIAA Atmospheric Flight Mechanics Conference and Exhibit*, American Institute of Aeronautics and Astronautics, 2001. doi:10.2514/6.2001-4072.

[12] Ohme, P., "A Model-Based Approach to Aircraft Takeoff and Landing Performance Assessment," *AIAA Atmospheric Flight Mechanics Conference*, American Institute of Aeronautics and Astronautics, 2009. doi:10.2514/6.2009-6154.

[13] Takahashi, T. T., and Delisle, M., "(Un)stabilized Approach - An Introduction to Dynamic Flight Conditions during Takeoff and Landing Climb," *2018 Aviation Technology, Integration, and Operations Conference*, American Institute of Aeronautics and Astronautics, 2018. doi:10.2514/6.2018-3500.

[14] Masson, B., Bain, M., and Page, J., "Engine-Out Takeoff Path Optimization out of Terrain Challenging Airports," *AIAA Guidance, Navigation, and Control Conference*, American Institute of Aeronautics and Astronautics, 2011. doi:10.2514/6.2011-6313.

[15] Talgorn, B., Laporte, S., Bes, C., and Segonds, S., "One Engine Out Takeoff Trajectory Optimization," *10th AIAA Aviation Technology, Integration, and Operations (ATIO) Conference*, American Institute of Aeronautics and Astronautics, 2010. doi:10.2514/6.2010-9013.

[16] Balachandran, S., and Atkins, E. M., "Flight Safety Assessment and Management for Takeoff Using Deterministic Moore Machines," *Journal of Aerospace Information Systems*, Vol. 12, No. 9, 2015, pp. 599–615. doi:10.2514/1.i010350.

[17] Koolstra, H. J., Huijbrechts, E.-J., and Mulder, J. A., "Analyzing Aircraft Controllability After Engine Failure During Takeoff in Adverse Weather Conditions," *Journal of Aircraft*, Vol. 56, No. 4, 2019, pp. 1330–1341. doi:10.2514/1.c035219.

[18] MAYNE, D., "A Second-order Gradient Method for Determining Optimal Trajectories of Non-linear Discrete-time Systems," *International Journal of Control*, Vol. 3, No. 1, 1966, pp. 85–95. doi:10.1080/00207176608921369.

[19] Xie, J., Chakraborty, I., Briceno, S. I., and Mavris, D. N., "Development of A Certification Module for Early Aircraft Design," *AIAA Aviation 2019 Forum*, American Institute of Aeronautics and Astronautics, 2019. doi:10.2514/6.2019-3576.

[20] Mistry, M., "Robot Learning and Sensorimotor Control," Nonlinear Optimal Control Lecture Note, Feb. 2018. URL http://wcms.inf.ed.ac.uk/ipab/rlsc/lecture-notes/RLSC-MM-04.pdf.

[21] Kirby, M. R., and Mavris, D., "The environmental design space," *26th international congress of the aeronautical sciences*, Vol. 26, Citeseer, 2008, pp. 2008–4.

[22] *737 Airplane Characteristics for Airport Planning*, Boeing Commercial Airplanes, Sep. 2013. URL http://www.boeing.com/assets/pdf/commercial/airports/acaps/737.pdf.

[23] Drela, M., and Youngren, H., *AVL 3.36 User Primer*, MIT, Feb. 2017.

[24] Mavris, D. N., and Schutte, J. S., "Application of Deterministic and Probabilistic System Design Methods and Enhancements of Conceptual Design Tools for ERA," Tech. rep., Georgia Institute of Technology & NASA Langley Research Center, 2016.